Proceedings World Geothermal Congress 2023
Beijing, China, April 17 – 21, 2023

Study on the hydraulic performance of geothermal electric submersible pump under gas-liquid flow

Ruixia Li[1,2], Ziwei Qi[1], Tianren Wang[2], Yongxue Zhang[1], Zhiyi Yuan[1], Zhongli Ji[1], Feng Chen[1]

1. College of Mechanical and Transportation Engineering, China University of Petroleum, Beijing 102249, China

2. Sinopec Star (Beijing) New Energy Research Institute Co., Ltd., Beijing 100083, China

Mailing Address: 18 Fuxue Road, Changping District, Beijing 102249, China

E-mail: risa2003@126.com

Keywords: Electric submersible pump; Geothermal wells; Entropy production analysis; Gas-liquid flow

ABSTRACT

Electric submersible pumps (ESP) are important devices for lifting geothermal water from geothermal wells to the ground. Due to the extreme environment and large flow characteristics of pump operation, the operation stability of the pump has become the focus of research. In this paper, the numerical simulation method was used to study the hydraulic performance of the two-stage geothermal well electric submersible pump under different air inlet conditions. Combined with the two-phase flow entropy production diagnostic method, the distribution and causes of hydraulic loss are studied. The study found that with the increase of air intake, the pump pressurization performance decreased significantly when a surge occurred. The inlet and outlet of the impellers and diffusers are the areas with the most serious severe hydraulic loss. In the inlet and outlet area of impellers, the change of the relative liquid flow angle caused by the two-phase flow leads to a significant increase in loss. Turbulent dissipation is also enhanced due to the generation of intense passage vortices and wake vortices of gas-liquid flow.

1. INTRODUCTION

Geothermal energy is the natural thermal energy from the lava inside the earth, which is a kind of abundant and renewable clean energy. As the main method of geothermal energy development and utilization, geothermal heating has been developing rapidly in recent years for the advantages of stability and continuity, high utilization efficiency, and low production cost (Rubio-Maya et al.,2015). The electric submersible pump is the key equipment for collecting geothermal water from geothermal wells to the ground, and its performance will directly affect the cost of production. Novotny et al. (2020) found that gas often exists in geothermal water, which will damage the pressurization performance of the pump, leading to safety problems, economic losses and other adverse effects. Therefore, it is vital to study the internal flow characteristics of the electric submersible pump under the mixed gas-liquid transport condition to improve the system operation performance, safety, reliability and the design theory of submersible pumps.

In recent years, scholars have studied the performance of gas-liquid two-phase flow in electric submersible pumps. Zhang et al. (2016) characterized four different flow patterns in a rotodynamic multiphase pump by visualization experiments: isolated bubbles flow, bubbly flow, gas pocket flow and segregated gas flow. Ali et al. (2021) found that when the pump was operating under gas-liquid two-phase flow conditions, the participation of gas and bubble size distribution would lead to the decline of pump performance, from slight deterioration to severe deterioration (surge and cavitation formation), and may lead to the gas completely blocked the flow passage (air lock). Shi et al. (2018) concluded that in the numerical simulation of gas-liquid two-phase flow in the pump, the SST turbulence model could sufficiently predict the flow field inside the impeller and identify the reflux area near the front cover plate of the impeller. Gamboa(2012) identified the initiation of the surging as the boundary between two performance regimes: one with a normal pump performance, in which the pressure increment increases as the liquid flow rate is reduced, and another where the pump pressure increment reduces with the decrease of the liquid flow rate. Zhu et al. (2017) and Zhu et al. (2019) concluded that the Eulerian-Eulerian multiphase model is superior to the VOF model in the simulation of gas-liquid two-phase flow in submersible pump. The gas phase is prone to gather near the leading edge, trailing edge and pressure side of the impeller blade. With the increase of inlet gas volume fraction (IGVF), the gas will accumulate and form air pockets, and the internal flow pattern transition will lead to different degrees of changes in the pressurization performance of the electric submersible pump.

Vortex is a typical flow structure in hydraulic machinery. Many researchers (Zhang et al., 2017a; Zhang et al. 2017b; Li et al., 2018a; Li et al., 2018b) found that the existence of vortex will increase hydraulic loss, aggravate pressure fluctuation, pump cavitation, increase pump vibration and noise, rotating stall and other instability problems. Therefore, accurate identification of vortex structure is of great significance for understanding the turbulent flow mechanism and solving the problem of hydraulic and mechanical instability. Today, the existing vortex identification methods include the Q criterion by Hunt (1988), Δ criterion by Chong et al. (1990), $\lambda 2$ criterion by Jeong and Hussain (1995) and Omega vortex identification method by Liu et al. (2016). Lin et al. (2018) and Lu et al. (2022) extracted the vortex structure in the flow field of mixed flow pump and centrifugal pump by using the Q criterion and pointed out that the internal vortex structure of the guide is mainly channel vortex and trailing edge shedding vortex, the channel vortex will always migrate with the flow to draft pipe. The rotor-stator interference between the rotating impeller and the static volute produces a large area of backflow and secondary flow at the volute edge and tongue, leading to hydraulic loss.

With the continuous improvement of entropy production theory, it has been widely used in fluid machinery. Research through Zhou et al. (2022) shows that compared with the traditional hydraulic loss evaluation method, the entropy production analysis method has the advantage that it can describe the distribution law of the irreversible loss in hydraulic machinery not only intuitively and accurately

but also quantitatively analyze the magnitude of the internal hydraulic loss. Application of the two-phase flow entropy production theory are also studied in recent years(Li et al., 2017; Guan et al., 2020; Zhou et al., 2022). Bilicki et al. (2002) deduced the two-phase entropy production theory based on the homogeneous model. Based on Bilicki, Wang et al. (2019) simplified Bilicki's entropy production model, and proposed a new two-phase flow entropy production model. It is verified that the model can sufficiently predict the gas-liquid interaction in the rotating machinery and its influence on the flow structure (Wang et al., 2020a; Wang et al., 2020b; Hang et al. 2022).

In summary, the study of gas-liquid two-phase flow in electric submersible pump mainly focuses on the influence of gas-liquid two-phase interaction on the flow structure. The quantity and distribution of energy loss caused by the change of IGVF is intuitively and accurately obtained. In addition, the vortex research and entropy production analysis in the two-phase flow of electric submersible pumps are not sufficient. Therefore, the Omega vortex identification method and two-phase entropy production diagnostic model were used in this paper to study the flow characteristics of the gas-liquid two-phase flow field in the electric submersible pumps, through the analysis of the vortex structure change and entropy production distribution law in gas intake conditions, the causes of hydraulic loss and key loss areas of ESP are obtained.

2. PHYSICAL MODELS AND NUMERICAL METHODS

2.1 Computational model

The single-stage 3D model of the submersible pump with the same geometrical parameters as mentioned above is shown in Fig. 1. To ensure the full development of inlet and outlet flows, the inlet and outlet pipes are extended to at least 4 times the hydraulic diameter. The main nominal parameters are listed as follows: the speed n is 2875 r/min; the designed flow rate Q_{des} is 125 m^3/h; the designed head of single stage H_{des} is 16 m. The geometrical parameters of the impeller and diffuser are shown in Table 1.

Table 1
Geometric structure parameters of impeller and diffuser.

Parameters	Impeller		Diffuser		Units
	Symbols	Values	Symbols	Values	
Hub diameter	$d_{Imp,h1}$	36	$d_{Diff,h2}$	36	mm
Inlet diameter	$d_{Imp,s1}$	98	$d_{Diff,s1}$	210	mm
Outlet diameter	$d_{Imp,h2}$	154	$d_{Diff,s2}$	98	mm
Blade inlet angle	$\beta_{Imp,1}$	24	$\beta_{Diff,1}$	26	°
Wrap angle	φ_{Imp}	110	φ_{Diff}	90	°
Blade outlet angle	$\beta_{Imp,2}$	30	$\beta_{Diff,2}$	90	°
Axial length	L_{Imp}	51	L_{Diff}	113	mm
Blade numbers	Z_{Imp}	7	Z_{Diff}	8	-

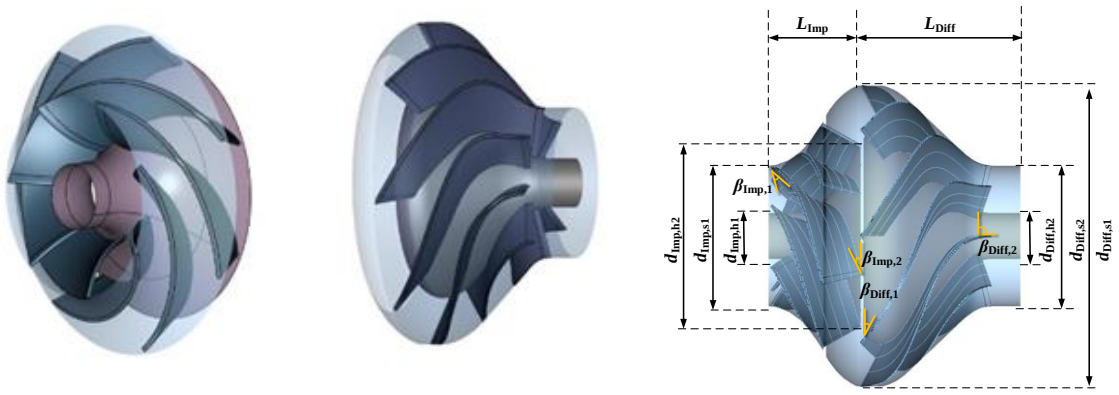

(a) (b) (c)

Figure 1: 3D diagram of the Electric submersible pump, (a) impeller, (b) diffuser, (c) main geometrical parameters of the impeller and diffuser.

2.2 Mesh sensitivity analysis

The calculation model of the two-stage submersible pump consists of inlet, impellers, diffusers and outlet, as shown in Fig. 2. Turbogrid and ICEM are applied to generate the structured meshes of the computational domain, such as impellers, diffusers, and inlet/outlet extension section. The grid aspect ratio is strictly controlled to ensure that the blade surface Y+ is less than 10, which meets the requirements of the turbulence model, as shown in Fig. 2.

The mesh independence analysis is carried out in the computational domain to reduce or eliminate the influence of the number of mesh elements on the calculation results. Five sets of refined meshes are generated to perform the mesh independence check. According to Table 2, when the mesh elements are larger than 7231622, the change in the head and efficiency are less than 1%. Thus, the number of meshes (7231622) is chosen for the following measurements.

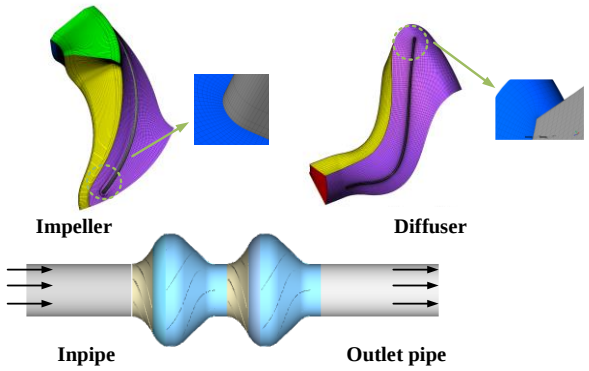

Figure 2: two-stage electric submersible pump model.

Table 2
Mesh scheme information and performance calculation comparison.

Mesh scheme	Elements	Head *H*/m	Error of head/%	Efficiency η/%	Error of Efficiency/%
1	3852698	42.7896	3.17	80.12	2.32
2	5625455	42.5863	2.68	79.56	1.61
3	6280196	42.4727	1.61	79.22	1.17
4	7231622	41.7989	0	78.30	0.00
5	10353302	41.9018	0.25	78.23	-0.09

2.3 Numerical settings

The 3D steady and transient gas-liquid two-phase simulations in the electric submersible pumps are conducted using the commercial CFD solver Fluent. The Euler-Euler two-fluid model is employed to solve the multiphase flow fields. Two sets of governing equations based on the Reynolds-averaged Navier–Stokes (RANS) method consisting of mass and momentum conservation equations are solved separately for the liquid phase and gas phase, and the shear stress transport (SST) k-ω turbulence model was selected. The SIMPLE algorithm is used to solve the pressure-velocity coupling equations, and the first-order upwind is selected as the differential equation. The boundary conditions of velocity and outflow are configured at the inlet and outlet, respectively. For solid walls, no-slip boundary conditions are applied. The impeller domain is simulated using a rotational frame, and the other domains are stationary. The calculation is converged if the root-mean-square (RMS) residual falls below 1.0×10^{-4}. The results of steady simulations are used as the initial conditions in transient calculations. The time-step of 5.78×10^{-5} s (equals the time of blade passing 1°) is selected. Normally, 20 iterations are needed to guarantee the convergence. In this paper, the first six revolutions are simulated, but the last four are used for data processing due to relatively stable flow fields.

2.4 Mathematical model

2.4.1 Eulerian-Eulerian mode

The Eulerian multiphase flow model is the most extensively applied method in calculating gas-liquid two-phase flow (Hang et al., 2022; Wang et al., 2020). Generally, water is the continuous phase, and gas is the discrete phase.

$$\alpha_g = \frac{Q_g}{Q_g + Q_l} \tag{1}$$

$$\alpha_g + \alpha_l = 1 \tag{2}$$

Where Q_g is the gas volume flow rate, Q_l is the liquid volume flow rate, α_g is the gas volume fraction and α_l is the liquid volume fraction. The continuity equation is as follows:

$$\frac{\partial}{\partial t}\left(\alpha_{\mathrm{m}}\rho_{\mathrm{m}}\right)+\nabla\cdot\left(\alpha_{\mathrm{m}}\rho_{\mathrm{m}}\boldsymbol{w}_{\mathrm{m}}\right)=0 \tag{3}$$

The momentum equation takes the following term:

$$\frac{\partial}{\partial t}\left(\alpha_m\rho_m\boldsymbol{w}_m\right)+\nabla\cdot\left(\alpha_m\rho_m\boldsymbol{w}_m\boldsymbol{w}_m\right)=-\alpha_m\nabla p_m+\nabla\cdot\left(\alpha_m\mu_m\left(\nabla\boldsymbol{w}_m+\left(\nabla\boldsymbol{w}_m\right)^T\right)\right)+\boldsymbol{M}_{\mathrm{m}}+\boldsymbol{F}_{\mathrm{m}} \tag{4}$$

where the subscript $m = g$ or l for gas and liquid. ρ is density, kg/m^3; α is volume fraction; p is pressure, Pa; μ is dynamic viscosity, Pa·s; w is relative fluid velocity, m/s; $\boldsymbol{M}$ is the interfacial force, N. $\boldsymbol{F}$ is the mass force associated with impeller rotation, N.

2.4.2 Omega vortex identification method

The Omega vortex identification method was proposed by Liu et al. (2016). Based on the idea of splitting vorticity into rotational part and non-rotational part, a parameter Ω is introduced to represent the relative rotational strength. The equations are as follows:

$$\nabla V=\frac{1}{2}\left(\nabla V+\nabla V^T\right)+\frac{1}{2}\left(\nabla V-\nabla V^T\right)=\boldsymbol{A}+\boldsymbol{B} \tag{5}$$

$$a=trace\left(\boldsymbol{A}^T\boldsymbol{A}\right)=\sum_{i=1}^{3}\sum_{j=1}^{3}\left(\boldsymbol{A}_{ij}\right)^2 \tag{6}$$

$$b=trace\left(\boldsymbol{B}^T\boldsymbol{B}\right)=\sum_{i=1}^{3}\sum_{j=1}^{3}\left(\boldsymbol{B}_{ij}\right)^2 \tag{7}$$

$$\Omega=\frac{b}{a+b+\varepsilon} \tag{8}$$

where $\boldsymbol{A}$ is symmetric tensor and $\boldsymbol{B}$ is anti-symmetric tensor. ε is set to ensure that the denominator does not equal 0.

2.4.3 The two-phase flow entropy production model in the electric submersible pump

To better understand the multiphase flow mechanism inside the electric submersible pump, the entropy production diagnostic model is employed in this paper, which can describe the flow characteristics in detail by analyzing the local energy loss under two-phase flow. The total entropy production rate can be divided into three items:

Direct entropy production rate:

$$\dot{P}_D=\frac{2\mu_m}{\bar{T}}\left\{\left(\frac{\partial\bar{v}_x}{\partial x}\right)^2+\left(\frac{\partial\bar{v}_y}{\partial y}\right)^2+\left(\frac{\partial\bar{v}_z}{\partial z}\right)^2\right\}+\frac{\mu_m}{\bar{T}}\left\{\left(\frac{\partial\bar{v}_x}{\partial y}+\frac{\partial\bar{v}_y}{\partial x}\right)^2+\left(\frac{\partial\bar{v}_x}{\partial z}+\frac{\partial\bar{v}_z}{\partial x}\right)^2+\left(\frac{\partial\bar{v}_y}{\partial z}+\frac{\partial\bar{v}_z}{\partial y}\right)^2\right\} \tag{9}$$

Turbulent entropy production rate: $\dot{P}_T=\frac{\rho_m\varepsilon_m}{T}=\frac{\rho_m\omega_m k_m}{T}$ (10)

Wall entropy production rate: $\dot{P}_W=\frac{\boldsymbol{\tau}_{W,i}v_i}{T}$ (11)

where '-' means the time-averaged values, $\boldsymbol{\tau}_{w,i}$ is the wall shear stress and $\boldsymbol{v}_i$ is the mean velocity at the first-layer grid near the wall. The temperature T approximately keeps a constant of T = 298 K, v_m is the mixture velocity obtained by the weighted average of gas-liquid velocity. $\boldsymbol{\tau}_w$ is the wall shear stress tensor. ε is turbulence eddy dissipation rate.

The total entropy production rate can be integrated by:

$$\int_V\dot{P}_s\,dV=\int_V\dot{P}_D dV+\int_V\dot{P}_T dV+\int_A\dot{P}_W dA \tag{12}$$

2.5 Simulation validation

As presented in Fig. 3, the experimental test facility comprises a liquid and gas circulation pipeline. The design rotational speed n = 1450 r/min, the design flow rate Q_0 = 6.25 m^3/h.

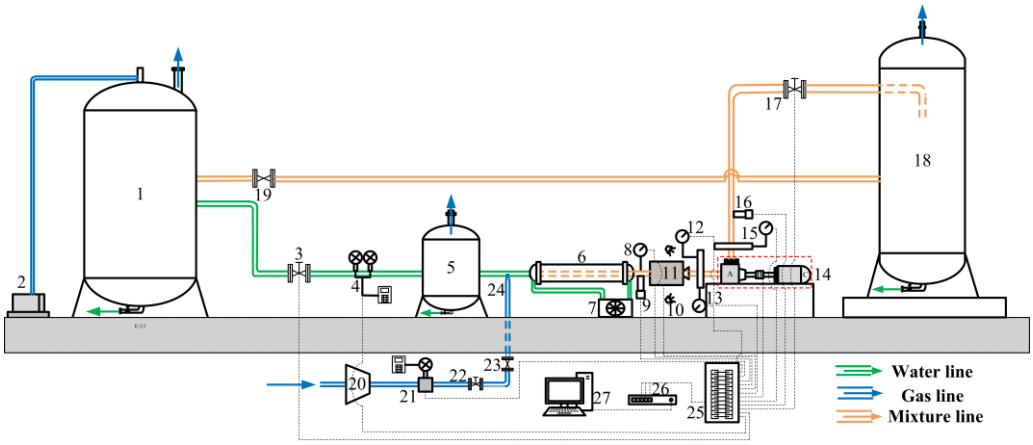

Figure 3: Schematic of the testing facility: 1-liquid tank, 2-water ring vacuum pump, 3-inlet motorized gate valve, 4-ultrasonic flowmeter, 5-steady-flow tank, 6-heat exchange, 7-thermo-chiller, 8-temperature sensor, 9-inlet hydrophone, 10-light source, 11-high speed CCD camera, 12-inlet pressure difference sensor, 13-electric-contact pressure gauge, 14-centrifugal pump system, A-centrifugal pump, B-torque transducer, C-electric motor, 15-outlet pressure difference sensor, 16-outlet hydrophone, 17-outlet motorized gate valve, 18-surge tank, 19-check valve, 20-compressor, 21-air tank, 22-air mass flowmeter, 23-needle valve, 24-check valve, 25-air injection nozzle, 26-data acquisition panel, 27-synchronous trigger, 28-computer.

The pump model of Wang et al. (2020) is used to verify the reliability of the SST turbulence model and Euler–Euler model. In Figure 4, the trends of the experimental and simulation results are consistent. The error under different IGVF is less than 3.6%, so it can be considered that the simulation method selected in this paper is reliable, which lays a foundation for further analysis of entropy production distribution and vortex in the pump under gas-liquid two-phase flow.

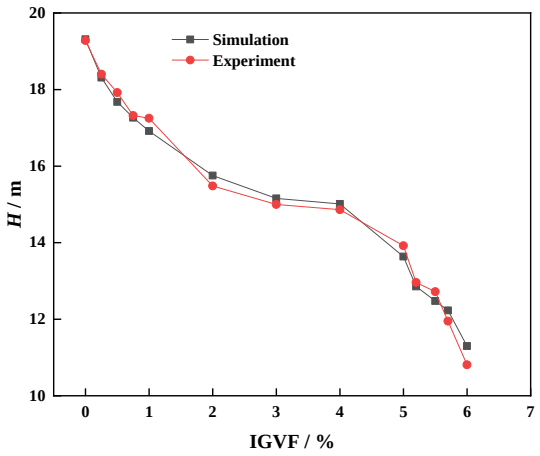

Figure 4: Performance curves from experiments and numerical simulations

3. RESULTS AND DISCUSSIONS

3.1 Effect of IGVF on the performance of ESP

The relationship between IGVF and performance deterioration of ESP is discussed. In Fig. 5. With the increase of air content at the inlet, the pressure difference between the inlet and outlet of the pump gradually decreases. Under the condition of low inlet gas content, the rate of decline in pump performance is small. However, when the IGVF is higher than 5%, the pump pressure suddenly drops, forming a significant inflection point. Zhu et al. (2017) suggested that this is the surging initiation region, which causes strong vibration and noise. The gas lock phenomenon is expected if the IGVF is further increased until the pressure increment is almost zero.

Comparing the entropy production loss of each component under different IGVF in Fig. 6. The results show that the difference between the entropy production rate of the diffusers and impellers is relatively small in the state of no air intake. With the increase of the inlet air volume, the entropy production rate of the impeller gradually increases and the entropy production rate of the diffusers shows a trend of decreasing and then increasing. For the whole flow passage, the total entropy production rate shows the rule of first increasing, then decreasing, and finally increasing. The result is the same as the experiment of (Wang et al., 2020), which shows that the internal hydraulic loss of the difffuser changes with the increase of IGVF. In the surging initiation region, the loss is mainly in the impeller, and the entropy production inside the diffuser is reduced. It shows that the impact on the impellers' internal flow field is severe when surging occurs. On the one hand, the flow pattern changes, and the gas gathers inside the impeller, blocking the flow channel and causing flow disturbance, resulting in increased entropy production. On the other hand, as the gas volume fraction increases, which will affect the liquid flow state at the impeller inlet and change the relative liquid flow angle, resulting in an increasing impact loss from the blade's leading edge. In addition, the turbulent dissipation is enhanced in the outlet area due to the shedding of the wake vortex, which causes the loss extremum area.

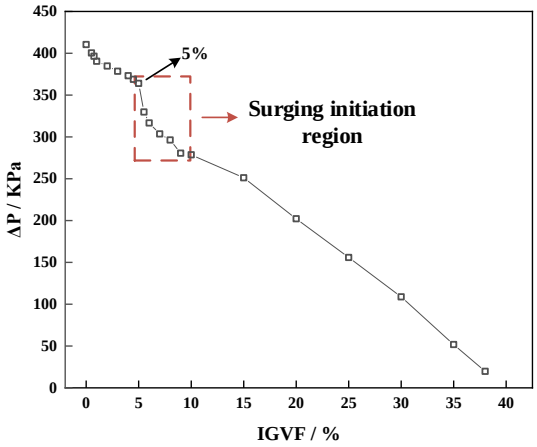

Figure 5: Effect of IGVF on the pressure increment at n = 2875 rpm, Q_l = 125 m^3/h.

According to the above analysis, The relationship between performance curve, entropy production rate and IGVF could be seen. To further discuss the factors affecting the performance of ESP under the condition of gas intake, To further discuss the factors affecting the performance of ESP under the condition of surging, the impeller blade inlet relative liquid flow angle, entropy production distribution of internal flow field and vortex structure will be investigated in depth.

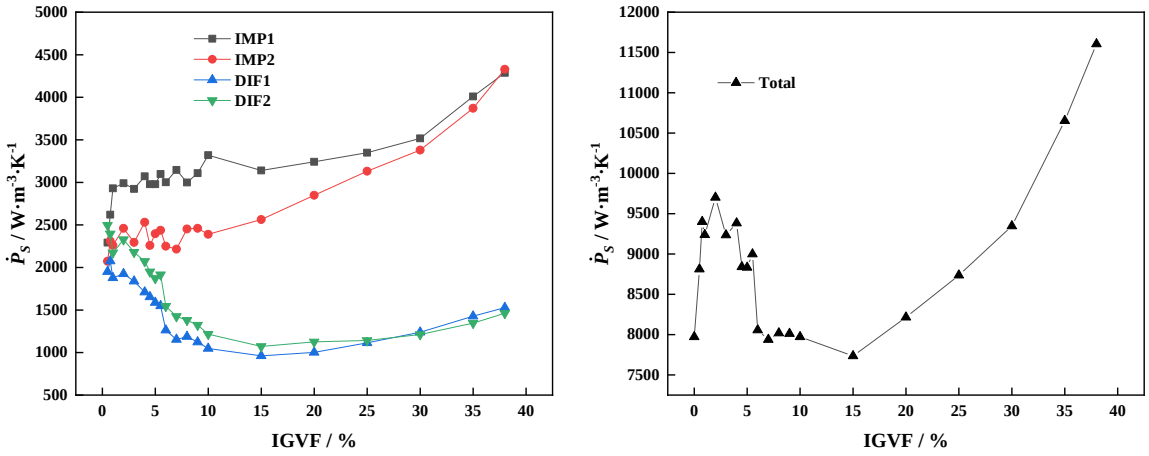

(a) **(b)**

Figure 6: Comparison of entropy production with different IGVF at n = 2875 rpm, Q_l = 125 m^3/h, (a) impellers and diffusers, (b) Entire ESP flow passage

3.2 Effect of gas content on the distribution of entropy production

The entropy production of the internal flow field and the change of the relative liquid flow angle of the electric submersible pump under the conditions of no air intake and the beginning of surging (IGVF=5%) are discussed. Fig. 7 illustrates the total entropy production distribution in ESP. As can be seen from the figure, With the gas enters the submerged pump, the hydraulic loss in the entire flow path increases. The area of the most severe energy loss is the trailing edge of the diffusers, the inlet and outlet of the impeller and diffusers. The entropy production in the flow path of the first stage impeller is relatively less (this is because the fluid flow is not yet fully developed in the first stage impeller). Combined with the specific distribution law of entropy production in the flow channel, it can visually identify the location of higher energy losses, which can provide a reference for the energy-saving optimization design of multistage electrical submersible pumps.

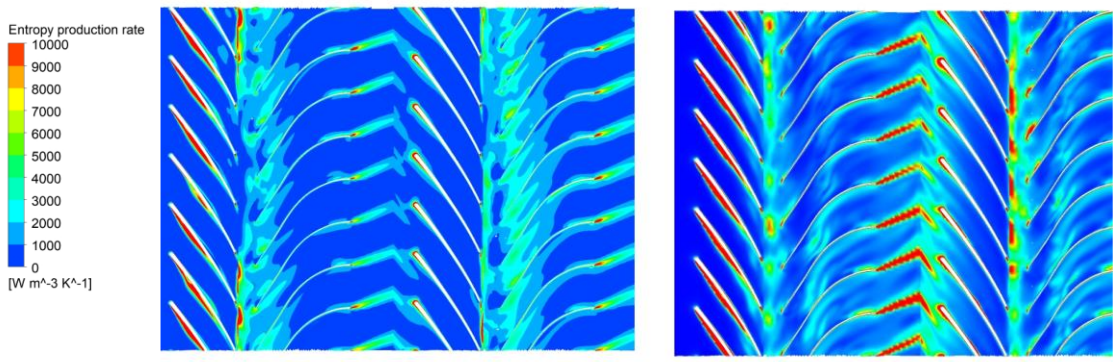

(a) IGVF = 0% **(b) IGVF = 5%**

Figure 7: Entropy production distribution in spanwise surfaces of ESP (span = 0.5).

Fig. 8 describes the velocity triangle on the meridional surface, where v_1 represents the absolute velocity, w_1 represents the relative velocity and u_1 is the peripheral velocity. v_{u1} is the relative velocity in the circumferential direction and v_{m1} is the absolute velocity in the meridional direction. To better understand the influence of the inlet relative liquid flow angle β_1' on the hydraulic losses of submersible pumps, the monitoring circle shown in Figure 9 is extracted to analyze the changes in relative liquid flow angle.

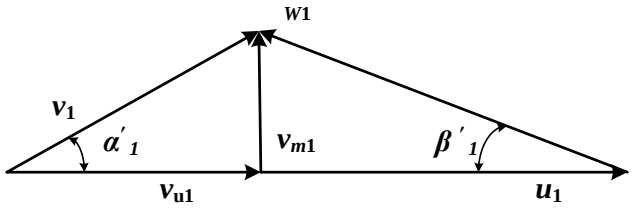

Figure 8: Velocity triangle and the relative liquid flow angle

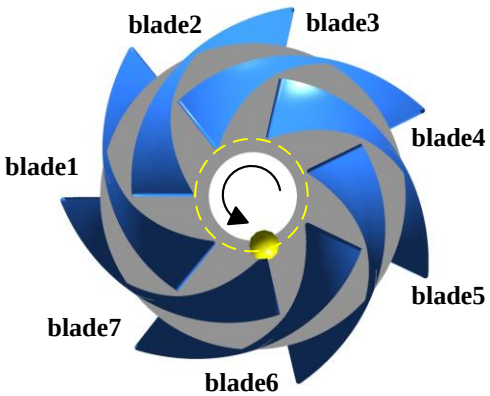

Figure 9: Circumferential starting point of impeller inlet

The relative velocity of the water flow at the inlet of the impeller is inconsistent with the tangent direction of the centerline of the impeller blade, which forms the flow angle of attack, leading to flow separation and vortex at the inlet area of the blade, resulting in impact loss. The decrease of the relative liquid flow angle at the pressure side of the blade and the increase of the relative liquid flow angle at the suction side of the blade will increase the energy loss. As can be seen from Fig. 10, with the circumferential position of impeller inlet changes, the relative liquid flow angle shows a periodic change. The relative liquid flow angle near the blade fluctuates significantly, causing severe impact loss. The change of the relative liquid flow angle at the inlet of the second stage impeller is more complex than that at the inlet of the first stage impeller. The change of the relative liquid flow angle in the channel will increase the turbulent dissipation. Under the condition of the air intake, the gas makes the inlet passage of the second stage impeller and the internal relative liquid flow angle increase at the inlet of the second stage impeller, and the relative liquid flow angle near the blade changes irregularly. However, the change of the relative liquid flow angle at the inlet of the first stage impeller is small, as the gas will complicate the flow state at the inlet of the second stage impeller (Hang et al., 2022).

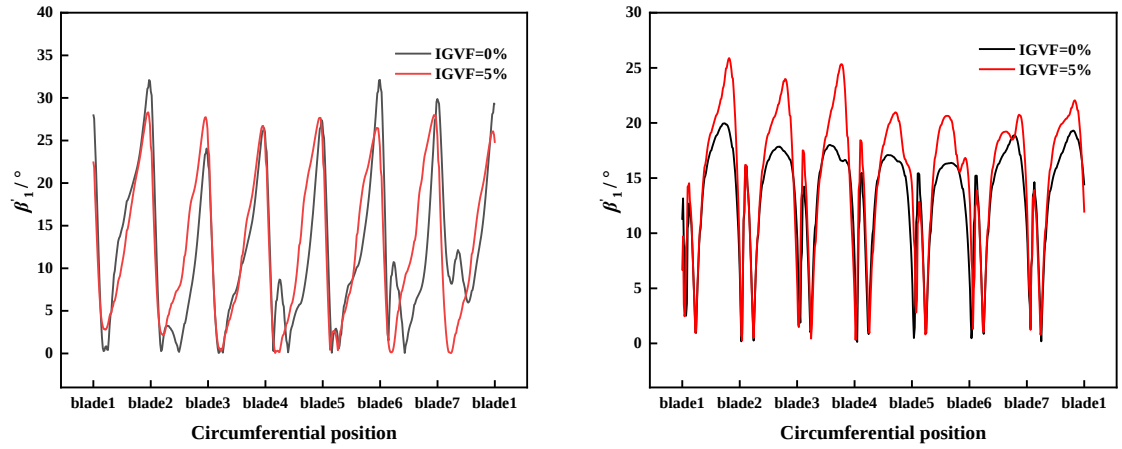

(a) 1st stage **(b) 2nd stage**

Figure 10: The relative liquid flow angle distribution of the impeller inlet.

In Figure 11, The relative liquid flow angle on the pressure side of the blade changes little, the change of the relative liquid flow angle is mainly concentrated on the suction side of the blade and inside the internal flow passage of impellers, changes of the relative liquid flow angle in the flow passage have little influence on the entropy production. The gas phase in the blade channel will extrude the liquid phase, resulting in deviation of the absolute velocity of the liquid phase at the blade wall, causing the change of the relative liquid flow angle near the blade, and the deterioration of the flow state in the channel.

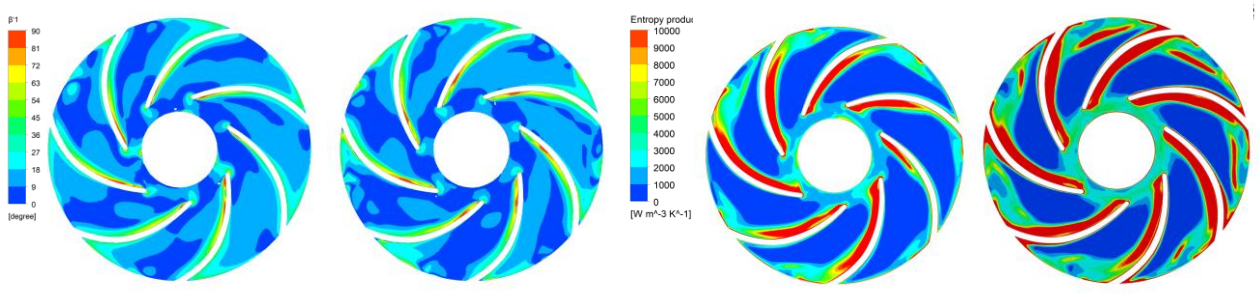

IGVF = 0% **IGVF = 5%** **IGVF = 0%** **IGVF = 5%**

(a) 1st stage

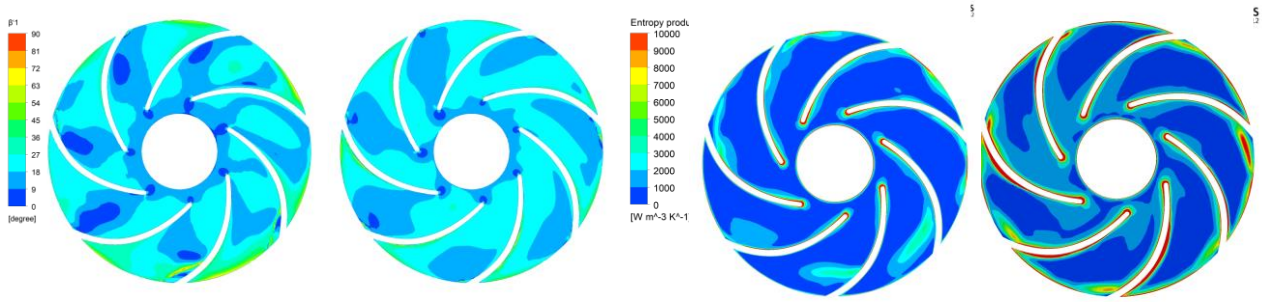

IGVF = 0% **IGVF = 5%** **IGVF = 0%** **IGVF = 5%**

(b) 2nd stage

Figure 11: Relative liquid flow angle and entropy production distribution in the impeller.

3.3 Vortex structures and irreversible losses

Combining with the entropy production analysis and the Omega identification method, the relationship between vortex structures and irreversible losses in instantaneous conditions is discussed. The velocity streamlines and the Omega contour of the first stage impeller and diffuser were made, as shown in Fig. 12. The backflow of flow separation phenomenon occurs at the impeller inlet, leading to the formation of many messy small vortex structures at the blade inlet. The vortices at the trailing edge of the impeller blade occupy a large area, and it will block the flow passage, affects the internal flow characteristics of the pump, and increases the flow dissipation, especially under the condition of gas-liquid flow. The vortices in the diffusers are mainly concentrated in the passage, which is affected by the impeller wake, and the rotor-stator interaction of the impeller and diffusers. The separation flow near the guide blade will increase the impact loss.

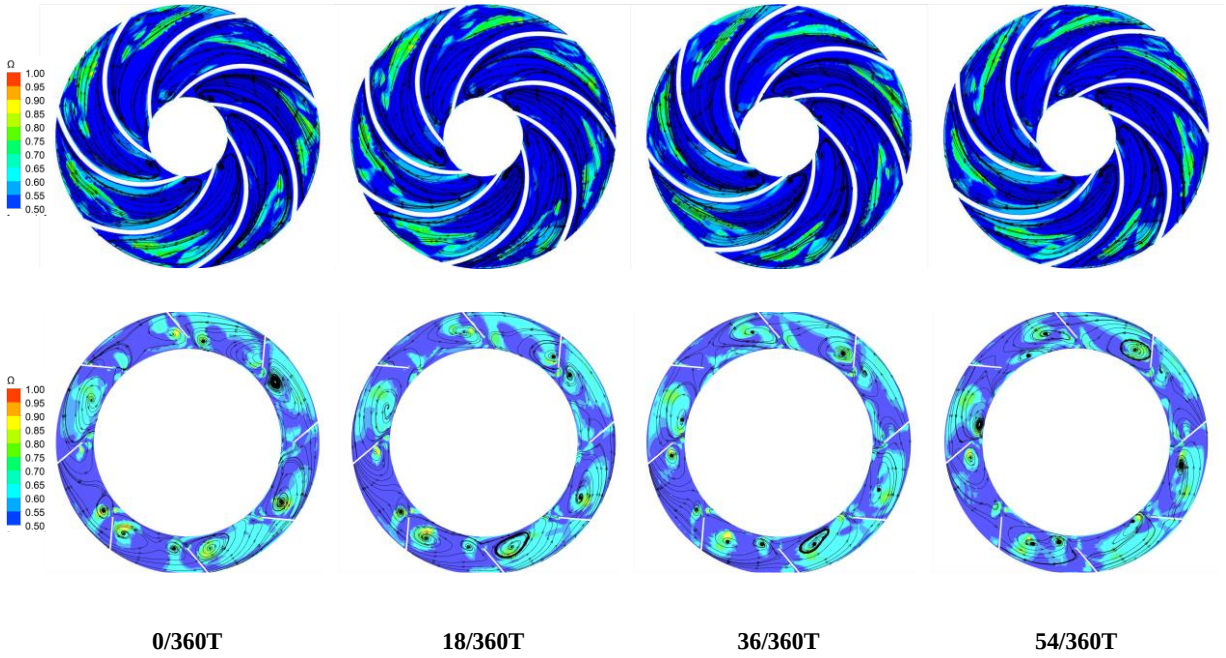

(a) IGVF = 0%

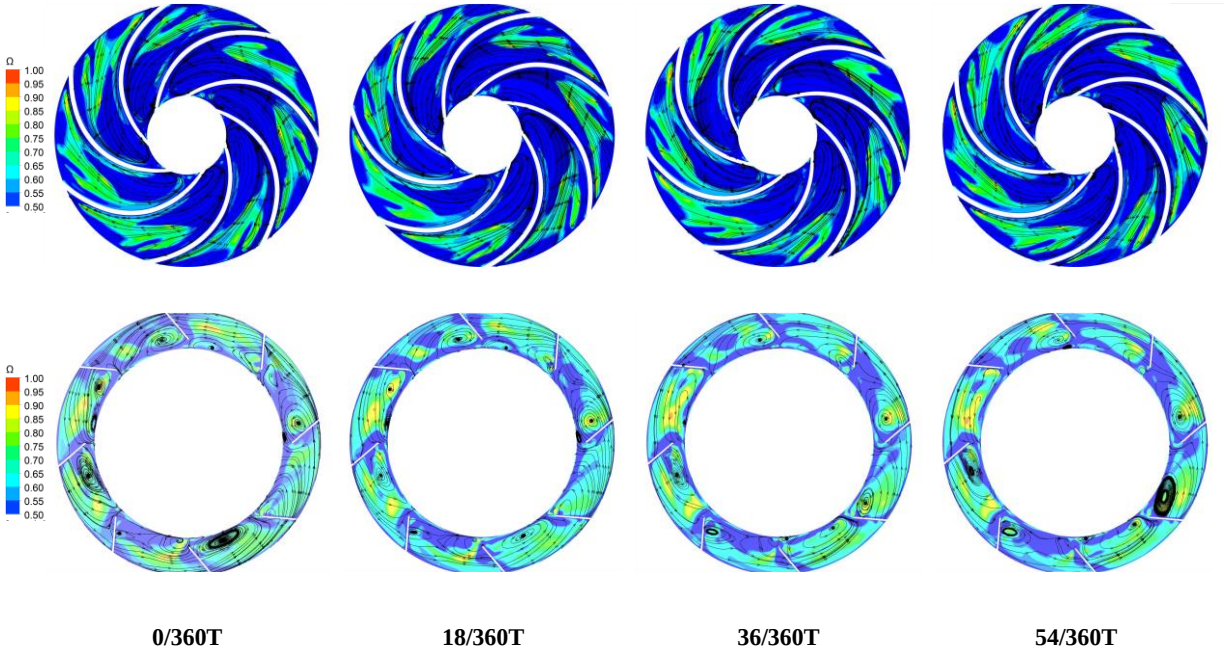

(b) IGVF = 5%

Figure 12: Temporal evolutions of instantaneous streamlines and omega of 1st stage impeller and diffuser

Fig. 12 and Fig. 13 depict the time evolution of the relationship between the internal vortex structure and entropy production distribution under design flow rate and the inlet gas volume fraction of 5%. It can be seen that the vortices at the trailing edge of the impeller blade increase first and then decrease. The same pattern can be seen at the inlet of diffuser. In Figure 13, it can be seen that the entropy production is larger in the area near the blade, the inlet and outlet area of the blade, which is the same as the previous analysis results. However, for the diffuser, the vortex in the flow channel increases and the entropy production decreases instead. This is because when the surging occurs, the gas gathers in the impeller and blocks the flow channel, resulting in a smaller velocity of the fluid flowing into the diffuser and a decrease in the turbulent entropy, which corresponds to the decrease in the entropy yield of the diffuser. Figure 5 also indicates that the gas tends to gather in the impeller under the gas intake conditions.

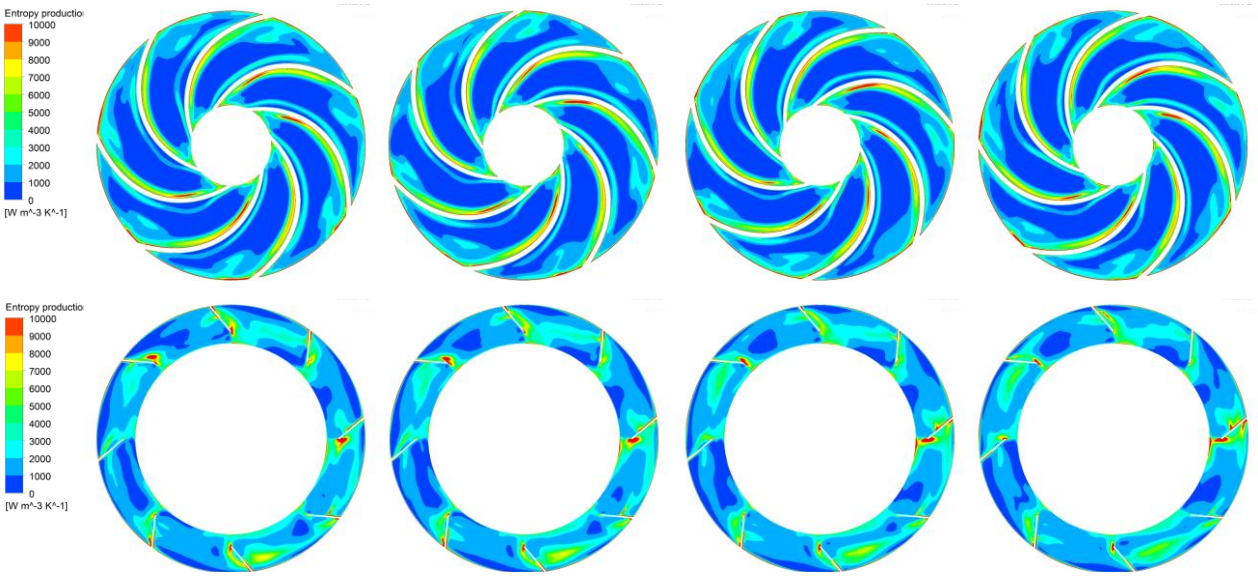

(a) IGVF = 0%

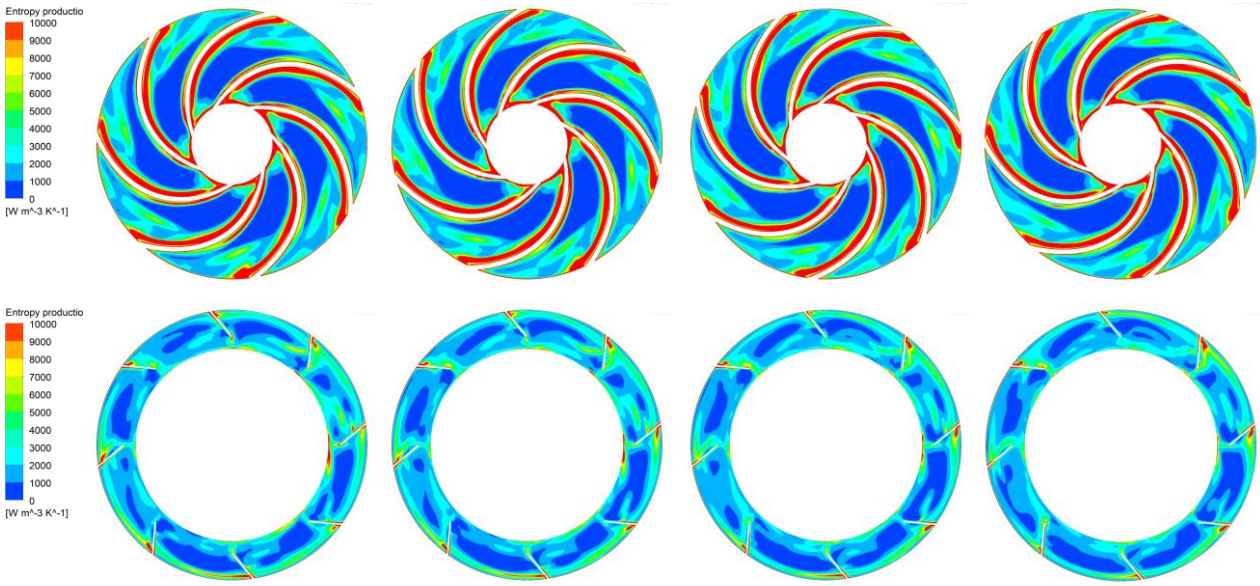

(b) IGVF = 5%

Fig. 13. 1st stage impeller and diffuser entropy production distribution

4. CONCLUSIONS

This paper studies the causes of hydraulic loss in the internal flow field of two-stage submersible pumps in geothermal wells under air intake conditions. The following conclusions are obtained through two-phase flow entropy production diagnosis and Omega vortex identification method.

(1) When ESP transports gas-liquid two-phase fluid, the gas is prone to gather in the first stage impeller. With the increase of the IGVF, the entropy production inside the diffuser first decreases and then increases. At the designed flow rate, the loss area of the internal flow field is mainly concentrated in the inlet and outlet area of the impellers and diffusers.

(2) The presence of gas will change the relative liquid flow angle inside the impeller, the blade inlet area of flow separation and vortex will cause impact loss. The increase of the relative liquid flow angle at the suction side of the blade will increase the impact loss. The influence of gas intake on the relative flow angle of the second impeller inlet is greater because the gas-liquid flow inside

the first impeller has not been fully developed, and the incoming flow of the second impeller is more complicated than that of the first impeller. The relative liquid flow angle change of the first-stage impeller outlet is more complicated than the second-stage impeller outlet, resulting in a greater entropy output of the first-stage impeller outlet than the second-stage impeller outlet and more severe hydraulic losses.

(3) The vortex structures in the submersible pump increase significantly under the gas-liquid flow. The passage vortex could block the flow channel and cause high loss. The turbulent dissipation is also enhanced in the outlet area due to the intense trailing vortices production under gas-liquid flow.

REFERENCES

Rubio-Maya C, Ambríz Díaz VM, Pastor Martínez E, Belman-Flores JM. Cascade utilization of low and medium enthalpy geothermal resources − A review. Renewable and Sustainable Energy Reviews. (2015):689-716.

Novotny V, Vitvarova M, Spale J, Jakobsen JP. Intermediate pressure reboiling in geothermal flash plant for increased power production and more effective non-condensable gas abatement. Energy Reports. (2020):20-7.

Zhang J, Cai S, Li Y, Zhu H, Zhang Y. Visualization study of gas–liquid two-phase flow patterns inside a three-stage rotodynamic multiphase pump. Experimental Thermal and Fluid Science, (2016):125-38.

Ali A, Yuan J, Deng F, Wang B, Liu L, Si Q, et al. Research Progress and Prospects of Multi-Stage Centrifugal Pump Capability for Handling Gas–Liquid Multiphase Flow: Comparison and Empirical Model Validation[J]. Energies. (2021):896.

Shi Y, Zhu H, Zhang J, Zhang J, Zhao J. Experiment and numerical study of a new generation three-stage multiphase pump. Journal of Petroleum Science and Engineering. (2018):471-84.

Gamboa JAMP. Experimental Study of Two-Phase Performance of an Electric-Submersible- Pump Stage. SPE Production & Operations. (2012): 27(04): 414-421.

Zhu J, Zhang H Q. Numerical Study on Electrical- Submersible-Pump Two-Phase Performance and Bubble-Size Modeling. SPE Production & Operations. (2017):267-78.

Zhu J, Zhu H, Zhang J, Zhang H. A numerical study on flow patterns inside an electrical submersible pump (ESP) and comparison with visualization experiments. Journal of Petroleum Science and Engineering. (2019):339-50.

Zhang Y, Chen T, Li J, Yu J. Experimental Study of Load Variations on Pressure Fluctuations in a Prototype Reversible Pump Turbine in Generating Mode. Journal of Fluids Engineering. (2017a).

Zhang Y, Zhang Y, Wu Y. A review of rotating stall in reversible pump turbine. Proceedings of the Institution of Mechanical Engineers, Part C: Journal of Mechanical Engineering Science. (2017b):1181-204.

Li D, Wang H, Qin Y, Wei X, Qin D. Numerical simulation of hysteresis characteristic in the hump region of a pump-turbine model. Renewable energy. (2018a):433-47.

Li X, Jiang Z, Zhu Z, Si Q, Li Y. Entropy generation analysis for the cavitating head-drop characteristic of a centrifugal pump. Proceedings of the Institution of Mechanical Engineers, Part C: Journal of Mechanical Engineering Science. (2018b):4637-46.

Hunt J C R WAA. Eddies, Streams, and Convergence Zones in Turbulent Flows. Studying turbulence using numerical simulation databases, 2. Proceedings of the 1988 summer program. (1988).

Chong MS, Perry AE, Cantwell BJ. A general classification of three‐dimensional flow fields. Physics of Fluids A: Fluid Dynamics. (1990):765-77.

Jeong J, Hussain F. On the identification of a vortex. Journal of Fluid Mechanics. (1995):69-94.

Liu C, Wang Y, Yang Y, Duan Z. New omega vortex identification method. Science China Physics, Mechanics & Astronomy. (2016).

Lin D, Su X, Yuan X. DDES Analysis of the Wake Vortex Related Unsteadiness and Losses in the Environment of a High-Pressure Turbine Stage. Journal of Turbomachinery. (2018):41001.

Lu J, Chen Q, Liu X, Zhu B, Yuan S. Investigation on pressure fluctuations induced by flow instabilities in a centrifugal pump. Ocean Engineering. (2022):111805.

Zhou L, Hang J, Bai L, Krzemianowski Z, El-Emam MA, Yasser E, et al. Application of entropy production theory for energy losses and other investigation in pumps and turbines: A review. Applied Energy. (2022):119211.

Guan H, Jiang W, Yang J, Wang Y, Zhao X, Wang J. Energy loss analysis of the double-suction centrifugal pump under different flow rates based on entropy production theory. Proceedings of the Institution of Mechanical Engineers, Part C: Journal of Mechanical Engineering Science. (2020):4009-23.

Li D, Wang H, Qin Y, Han L, Wei X, Qin D. Entropy production analysis of hysteresis characteristic of a pump-turbine model. Energy Conversion and Management. (2017):175-91.

Bilicki Z, Giot M, Kwidzinski R. Fundamentals of two-phase flow by the method of irreversible thermodynamics. International journal of multiphase flow. (2002):1983-2005.

Wang C, Zhang Y, Hou H, Zhang J, Xu C. Entropy production diagnostic analysis of energy consumption for cavitation flow in a two-stage LNG cryogenic submerged pump. International Journal of Heat and Mass Transfer. (2019):342-56.

Wang C, Zhang Y, Yuan Z, Ji K. Development and application of the entropy production diagnostic model to the cavitation flow of a pump-turbine in pump mode. Renewable energy. (2020a):774-85.

Wang B, Zhang H, Deng F, Wang C, Si Q. Effect of Short Blade Circumferential Position Arrangement on Gas-Liquid Two-Phase Flow Performance of Centrifugal Pump. Processes. (2020b):1317.

Hang J, Bai L, Zhou L, Jiang L, Shi W, Agarwal R. Inter-stage energy characteristics of electrical submersible pump under gassy conditions. Energy. (2022):124624.

Gamboa J, Prado M. Review of electrical-submersible-pump surging correlation and models[J]. SPE Production & Operations, (2011), 26(04): 314-324.

Zhu J, Guo X, Liang F, et al. Experimental study and mechanistic modeling of pressure surging in electrical submersible pump[J]. Journal of Natural Gas Science and Engineering. (2017), 45: 625-636.

Wang C , Zhang Y , Zhang J , et al. Flow pattern recognition inside a rotodynamic multiphase pump via developed entropy production diagnostic model[J]. Journal of Petroleum Science and Engineering. (2020), 194:107467.